Human Umbilical Cord Mesenchymal Stem Cell-derived Exosomal miR-27b Attenuate Subretinal Fibrosis via Suppressing Epithelial-mesenchymal Transition by Targeting HOXC6

dongli Li
Department of Ophthalmology,Shanghai General Hospital, Shanghai Jiao Tong University Schol of Medicine

Junxiu Zhang
Department of Ophthalmology,Shanghai General Hopsital, Shanghai Jiao Tong University School of Medicine

Zijia Liu
Department of Ophthalmology,Shanghai General Hospital,Shanghai Jiao Tong University School of Medicine

Yuanyuan Gong (gyydr@alumni.sjtu.edu.cn)
Shanghai Jiao Tong University School of Medicine

Zhi Zheng
Department of Ophthalmology,Shanghai General Hospital, Shanghai Jiaotong University School of Medicine

Research

Keywords: Epithelial–mesenchymal transition, exosomes, mesenchymal stem cells, subretinal fibrosis

Posted Date: November 2nd, 2020

DOI: https://doi.org/10.21203/rs.3.rs-99751/v1

Version of Record: A version of this preprint was published on January 7th, 2021. See the published version at https://doi.org/10.1186/s13287-020-02064-0.

Abstract

Background and aim

Subretinal fibrosis resulting from neovascular age-related macular degeneration (nAMD) is one of the major causes of serious and irreversible vision loss worldwide, and no definite and effective treatment exists currently. Retinal pigmented epithelium (RPE) cells are crucial in maintaining the visual function of normal eyes and its epithelial–mesenchymal transition (EMT) is associated with the pathogenesis of subretinal fibrosis. Stem cells-derived exosomes have been reported to play a crucial part in tissue fibrosis by transferring their molecular contents. This study aimed to explore the effects of human umbilical cord□derived mesenchymal stem cell exosomes (hucMSC-Exo) on subretinal fibrosis *in vivo* and *in vitro* and to investigate the anti-fibrotic mechanism of hucMSC-Exo.

Methods

In this study, we successfully cultured and identified human umbilical cord-derived mesenchymal stem cells (hucMSC), and isolated exosomes from their supernatant by ultracentrifugation.Laser-induced (choroidal neovascularization) CNV and subretinal fibrosis model indicated that intravitreal administration of hucMSC-Exo effectively alleviated subretinal fibrosis *in vivo*. Furthermore, we found that hucMSC-Exo could efficaciously suppress RPE cells migration and promote the mesenchymal–epithelial transition (MET) by delivering miR-27b-3p. Analysis of the latent binding of miR-27b-3p to HOXC6 was made by bioinformatics prediction and luciferase reporter assays.

Results

The study showed that intravitreal injection of hucMSC-Exo effectively ameliorated laser-induced CNV and subretinal fibrosis via suppression of EMT process. In addition, hucMSC-Exo containing miR-27b repressed the EMT process in RPE cells induced by the TGF-β2 via inhibiting HOXC6 (Homeobox protein Hox-C6) expression.

Conclusions

This study provided novel insights into the anti-fibrotic mechanism of hucMSC-Exo on subretinal fibrosis. HucMSCs-derived exosomal miR-27b could reverse the process of EMT induced by TGF-β2 via inhibiting HOXC6, which indicated that exosomal miR-27b/HOXC6 axis could play a vital role on ameliorating subretinal fibrosis. Our study put forward a promising therapeutic agent for the treatment of ocular fibrotic diseases, as well as comprehension into the mechanism of hucMSC-Exo under subretinal fibrosis.

Introduction

Subretinal fibrosis is a wound-healing response generated against CNV in nAMD responsible for severe blindness worldwide (1). In nAMD, CNV could stretch into Bruch's membrane or the retinal pigmented epithelium (RPE) layer, and subsequently form into a fibrovascular membrane, leading to retinal edema

and subretinal hemorrhage, causing the destruction of photoreceptors and RPE cells (2). RPE cells are the main contributor to fibrotic scars at the end of nAMD. During subretinal fibrosis secondary to neovascular AMD, RPE cells lose their characteristic epithelial morphology and function and then transform into myofibroblasts, which is called epithelial–mesenchymal transition (EMT). EMT is considered to be a key feature of pathological tissue that needs to be repaired in subretinal fibrosis (3).

Currently, the standard therapeutic modalities for nAMD is anti-vascular endothelial growth factor (VEGF) treatment. However, in the long run, frequent intravitreal administration of anti-VEGF drugs is not always able to successfully suppress the growth of CNV and its original efficacy will gradually decrease over time (4, 5). Several studies explained that anti-VEGFA treatment promotes the formation of fibrotic scars in the subretinal space, and fibrotic changes could reduce the efficacy of anti-VEGFA pathway(6-8). Therefore, the address of progressive fibrosis lesion including the reversal of EMT and the restoration of the epithelial phenotype will be potential molecular targets for neovascular AMD related subretinal fibrosis (9, 10).

Mesenchymal stem cells (MSCs) are one of the most widely used stem cell types for immunomodulation, organ reconstruction, and tissue repair in clinical practice(11). It has been reported that their leading role in tissue repair is mediated by paracrine action (12); Among these paracrine factors, exosomes are considered to be a novel treatment tool for delivering functional proteins, mRNA, miRNA and lncRNA (13).They are small membrane-bound particles, and may serve as a strong candidate for cell-free therapies on account of overcoming the limitations of cell-based therapy while maintaining the advantages of their original cells (14). In addition, exosomes are also ideal carriers and act as a crucial role in intercellular communication for the reason that the exosomal membrane can protect their molecular content from degradation before reaching the target cells (15).

Increasing studies have identified that exosomes secreted from MSCs could elicit significant therapeutic effects by suppressing fibrosis and improving their function in multiple-organ fibrosis models, such as liver, kidney, myocardium, and several retinal injury models (16-23). In addition, studies also reported that intravitreal injection of MSC-derived exosomes could ameliorate retinal laser injury by reducing damage, inhibiting apoptosis and inflammatory response (24). Treatment with MSC-derived exosomes retarded the growth of CNV and decreased the number of fibroblasts and collagen fibers after laser photocoagulation, indicating that MSC-derived exosomes have great potential to reduce collagen formation in subretinal fibrosis (19). Moreover, Mathew et al. proved that exosomes derived from MSCs with a intravitreal injection could keep in the vitreous humor over 4 weeks, combining with the vitreous proteins in a dose-dependent manner, indicating that administration of MSC-exosomes has a prolonged therapeutic effect and requires fewer injections (22).Based on the aforementioned finds, we believe that hucMSC-Exo could develop a cell-free regenerative therapy with great potential for treating subretinal fibrosis.

Materials And Methods

Ethics statement

All experiments on animals were approved by the Animal Care Committee of Shanghai General Hospital. Principles of animal research abided by the guidelines of ARVO Statement for the Use of Animals in Ophthalmic and Vision Research. The study was sanctioned by the Ethics Committee of the Shanghai General Hospital (Approval No.2020SQ120) and informed consents were acquired afore specimen collection.

Cell culture

Human skin fibroblasts (HSFs) and ARPE19 cells were all purchased from the American Type Culture Collection (USA). All above cells were maintained in Dulbecco's modified Eagle's medium (DMEM) and DMEM/Ham's F-12 medium (DMEM/F12, Gibco, USA) respectively. 10% fetal bovine serum (FBS)(Gibco, USA) and 1% penicillin/streptomycin were supplemented with cells at 37 °C with 5% CO2.

Preparation of hucMSCs

Briefly, fresh umbilical cords were obtained and washed with phosphate-buffered saline (PBS) containing 1% penicillin and streptomycin. Then, the blood vessels were taken out and the remaining tissue was cut into 1- mm^3 pieces on culture plates. The medium was replaced every 3 days. Nonadherent fragments were discarded, and the adherent cells were subcultured with 0.25% trypsin. The hucMSCs in passages 3–7 were used for further experiments.

The immune phenotype of hucMSCs was characterized by flow cytometry using a Human MSC Analysis Kit (562245; BD Biosciences, USA) which contained four positive markers (FITC-CD90, PerCP™Cy5.5-CD105, APC-CD73, and PE-CD44), five negative cocktails (PE-CD45, PE-CD34, PE-CD11b, PE-CD19, and PE-HLA-DR), and the respective isotype controls. The cells at a concentration of 5 × 10^6 cells/mL in PBS was stained following the BD's protocol. The analysis was carried out in a flow cytometer (Beckman Coulter, USA). Passage 3 hucMSCs were cultured in OriCell osteogenic and adipogenic differentiation media (Cyagen, Guangzhou, China) respectively as described by the manufacturer to identify the differentiation properties. After cultured for 23 days, hucMSCs were fixed and dyed with Alizarin red for osteogenic cells and Oil red for adipose cells. The cells cultured in a normal medium were served as controls.

Extraction and identification of hucMSC-derived exosomes

Exosome isolation was carried out following a previously published protocol(25) Briefly, hucMSCs were cultured and reached 50%–60% confluence. They were then placed in serum-free MSC medium (Nuwacell Biotechnology, RP02010-1 and RP02010-2, China). After 48 h of cultivation, the medium was obtained and centrifuged for 10 min at 300*g* and 30 min at 10000*g*. Next, the supernatant was filtered with a 0.22-μm filter (Millipore Corp, USA) and was further ultracentrifuged at 100,000*g* for 70min in a SW32Ti rotor (Beckman Coulter, USA). After removing the supernatant, the pellet was resuspended in PBS and then centrifuged at 100,000*g* for 70min again. Finally, the pellet was stored at -80℃ after being collected in 200-300uL of PBS .

The paiticle size distribution of hucMSC-Exo was analyzed using a nanoparticle tracking analysis system (ZetaView, Germany). Characteristic morphological observation of the exosomes was performed with a transmission electron microscope (FEI Tecnai Spirit G2). Western blotting was carried out to identify the expression of exosome-specific markers TSG101 (ab133586, Abcam, 1:1000 dilution), CD9 (A1703, Abclone, 1:1000 dilution), CD63 (25682-1-AP, Proteintech, 1:1000 dilution), and heat shock protein HSP70 (A12948, Abclone, 1:1000 dilution).

Exosome labeling

Purified exosomes were dyed with PKH67 (a green fluorescent dye; Sigma–Aldrich, Germany) following the instructions. Briefly, exosomes were stained with 4 μL of PKH67 in 200 μL of Diluent C fluid for 5 min. Next, an isovolumetric 1% BSA was appended to end the staining. PBS was used to wash the exosomes and re-purified via ultracentrifugation. Then, PKH67-labeled exosomes were incubated with ARPE19 cells for 12 h. Fluorescence microscopy (Leica Microsystems) was used to detect the green signals in cells.

Wound-healing assay

A total of 2×10^5 cells/well were plated and serum-starved overnight. Then, scratches on ARPE-19 cell monolayers were made with a sterilized 200-μL pipette tip. Images were recorded after 0, 24, and 48 h, and the wound recovery was analyzed using ImageJ. The migration capacity was determined by a percentage of wound closure.

Transwell assay

ARPE-19 cells (3×10^4) resuspended in 200 μL of serum-free medium were placed in the upper chamber with a polycarbonate membrane (8-μm pore size, Corning, USA). Then, 600 μL of DMEM/F12 supplemented with 10% FBS was added to the lower chamber. After incubation for 12 h, cells were stained with 0.1% crystal violet. For visualization, images of cultured cells were collected and counted in random different five fields.

Immunofluorescence staining

Birefly, cells after treatment were incubated with 1% BSA and 0.2% Triton X-100 for 2h. Then, the cells were co-cultivated with primary antibodies, namely, anti-alpha smooth muscle actin(anti-α-SMA) (#ab5694, Abcam, 1:100 dilution), anti-zonula occludens-1(anti-ZO-1) (#61-7300, Invitrogen, 1:50 dilution), and anti-Vimentin (#ARG66302, Arigo, 1:200 dilution, Shanghai) antibodies at 4°C. After that, cells was followed by incubation with the Cy3-conjugated donkey anti-rabbit IgG and the FITC-conjugated goat anti-mouse (Jackson ImmunoResearch Labs, USA) for 1 h.The nuclei were counterstained with DAPI (Beyotime, Shanghai) and the images were taken sequentially with a fluorescent microscope.

Western blot analysis

RIPA (Beyotime, China) supplemented with SDS buffer and protease inhibitors (Thermo Scientific) were used to extract total proteins. The proteins were transferred onto a PVDF membrane (Millipore, MA, USA) and then blocked with 5% skim milk. Primary antibodies against Vimentin (ARG66302, Arigo), α-SMA (ab5694, Abcam), occludin (SAB4200593, Sigma–Aldrich), and N-cadherin (13116, CST) were incubated with the membrane at 4°C overnight, with all of them were diluted at 1:1000. Next, cells were followed by incubation with a corresponding secondary antibody (HRP-conjugated goat anti-rabbit antibodies, 1:5000, ab15007).

Cells transfection with miRNA

Lipofectamine 2000 (Invitrogen, USA) was used for transfection. The cells were cultivated in six-well plates upon cell fusion of 60%. The instructions from GenePharma (Shanghai) were followed for the agomir and antagomir (100 pmol) transfection. The cells were harvested for the following efficiency and function assay 48 h after transfection.

RNA isolation and quantitation

We extracted total RNA from hucMSC-Exo using TRIzol Reagent (Takara, Japan). Before isopropanol precipitation, Dr.GenTLE Precipitation Carrier (#9094, TaKaRa,Japan) was added as a co-precipitant to increase the yield of exosomes RNA, which was reverse transcribed into cDNA with a Mir-X miRNA First-Strand Synthesis Kit (Cat. No. 638313, TaKaRa). qRT-PCR was performed using the TB Green Premix Ex Taq II (Tli RNaseH Plus) (RR820A, TaKaRa) and then detected with an ABI 7500 qPCR instrument (Thermo Fisher Scientific). The relative expression of miRNAs or mRNAs was analyzed using the $2^{-\Delta\Delta Ct}$ method. U6 or GAPDH were deemed as an internal control. The primer sequences were acquired from GenePharma (Shanghai) (Table 1).

Table 1.Primer sequences for real-time PCR

Primers	Sequences (5’ to 3’)
has-miR-100-5p	F’ AACCCGTAGATCCGAACTTGTG
has-miR-21-5p	F’ GCAGTAGCTTATCAGACTGATG
has-miR-27b-3p	F’ TTCACAGTGGCTAAGTTCTGC
has-miR-145-5p	F’ GGTCCAGTTTTCCCAGGA
has-miR-23b-3p	F’ AGATCACATTGCCAGGGA
has-miR-221-3p	F’ CAGAGCTACATTGTCTGCTG
has-miR-204-5p	F’ CAGTTCCCTTTGTCATCCTATG
has-miR-211-5p	F’ GCAGTTCCCTTTGTCATCCT
The 3’ primer for above Forward qPCR is the mRQ 3’ Primer, along with U6 Forward Primer and U6 Reverse Primer are supplied in Mir-X miRNA First-Strand Synthesis Kit (Cat. No. 638313)	

Dual-luciferase reporter assay

The cDNA of HOXC6 was loaded onto a psiCHECK2 vector (Promega, USA) (HOXC6- wild). Mutations are made in the potential miR-27b-3p-binding sites using a Fast Mutagenesis kit V2 (Vazyme, China) (HOXC6-mut). The luciferase activity was detected using a Dual-Luciferase Reporter Assay System (Promega,USA).

Laser-induced CNV model and drug administration

C57BL/6J mice aged 6–8 weeks were used in this study. All animals were housed at the Laboratory Animal Center of Shanghai General Hospital. The laser-induced subretinal fibrosis model was established as previously described and observed for 35 days to generate subretinal fibrosis(1). In brief, four to six laser spots (532 nm, 180 mW, 100 ms; Novus Spectra, Japan) were selected at each fundus around the optic disc. The disruption of Bruch’s membrane was confirmed by subretinal bubble formation immediately after laser application. HucMSC-Exo or PBS in 2 μL was injected into the vitreous cavity immediately after laser injury. After injection, the mice were randomly sacrificed (n = 15) on day 7, day 21, and day 35 for further quantification of CNV and subretinal fibrosis.

Choroidal flat-mount and immunofluorescence staining

The areas of CNV and collagen fibers were determined on choroidal flat mounts on day 7, day 21, and day 35. Mouse eyecups were fixed in 4% PFA, and anterior segments were removed before cutting four to six radial incisions to be flattened. Then, the RPE–choroid complexes were washed, blocked with 5% goat serum albumin and 0.3% Triton X-100, and then incubated with FITC-labeled isolectin-B4 (IB4) (Vector Laboratories, 1:100) (for evaluation of CNV) and collagen type I antibody (ab34710, Abcam, dilution

1:100) (for evaluating subretinal fibrosis) at 4°C overnight. The secondary antibody against collagen type I was Cy3-conjugated donkey anti-rabbit IgG (Jackson ImmunoResearch Labs, 1:200).

Hematoxylin and eosin and Masson staining

The eyes were removed after 7, 21, and 35 days and fixed for 2 h at 4°C in 4% PFA, then dehydrated and embedded in paraffin. Hematoxylin and eosin (H&E) staining was conducted following specific protocols. Masson's trichrome staining was carried out with a trichrome staining kit (ab150686, Abcam). The rate was automatically averaged using ImageJ (MD, USA).

Statistical analysis

GraphPad Prism Version 8.2 was used for statistical analysis. All data were expressed as mean ± standard deviation (SD). Statistical analysis between two sets of data was performed with the Student *t* test. Comparisons between multiple groups were analyzed by one-way analysis of variance. A *P* value less than 0.05 indicated a statistically significant difference.

Results

Isolation and identification of hucMSCs

HucMSCs were successfully isolated from Wharton's jelly region of umbilical cords. After culturing for two weeks, the cells around tissue blocks displayed a fibroblast-like morphology and attached to the plastic surface (Fig. 1a). After passage, they grew rapidly and arranged in a spiral pattern (Fig. 1b). MSCs could undergo differentiation to osteocytes and adipocytes and their multipotency property was detected by Oil red O staining (Fig. 1c, d) and Alizarin red respectively (Fig.1e, f). The expression of surface markers of hucMSCs was determined by flow cytometry. The positive markers of CD73, CD90, and CD105 along with negative cocktail markers (CD19, CD34, CD45, CD14, and HLA-DR) were shown in Figure.1g. Mouse isotypic IgG was used as a control. These results showed that hucMSCs were successfully isolated and identified.

Exosome purification, characterization, andinternalization into cells

HucMSC-Exo were purified from the third to seventh generation medium by serial centrifugation as described in Figure. 2a. As shown in Figure. 2b, the round or oval membranous vesicle morphology of exosomes was evaluated under a transmission electron microscope. Nanoparticle tracking analysis showed that the distribution of the particle size mainly focused on 30 to 160 nm particle size (Fig. 2c). Western blot analysis showed that traditional exosomal markers (CD9, TSG101, CD63, and HSP70) were expressed obviously in isolated hucMSC-Exo (Fig. 2d). Therefore, it was confirmed that hucMSC-Exo were isolated successfully. Furthermore, PKH67-labeled exosomes were observed under a confocal microscope. The result revealed that exosomes were internalized by ARPE19 cells and intensively distributed around the nucleus (Fig. 2e).

hucMSC-Exo alleviated laser-induced CNV and subretinal fibrosis in mice

To explore the anti-fibrotic influence of hucMSC-Exo on subretinal fibrosis in vivo, laser-induced CNV and subretinal fibrosis model was established and intravitreal injection was performed immediately (Fig. 3a). Masson staining performed on choroidal flat mounts revealed that obvious disruption change could observed in the choroidal layer and outer nuclear layers within the center of laser burn 7days after laser photocoagulation. Subsequently, newly formed vessels and retinal edema were discovered to be extended into the subretinal space 7days and 21 days after laser photocoagulation. The collagen area was obviously decreased in hucMSC-Exo group compared with control group after 21 and 35 days (Fig. 3b, $P < 0.05$). Furthermore, immunofluorescence staining of choroidal flat-mount indicated that the area of CNV was up to a maximum at day 7 and declined gradually between day 21 and day 35. Importantly, fewer vascular channels (isolectin-B4) and area of fibrosis (type 1 collagen) were observed in the subretinal space after 21 days in the hucMSC-Exo group (Fig. 3c, $P < 0.05$). These findings indicated that hucMSC-Exo strongly reduced laser-induced subretinal fibrosis in mice.

hucMSC-Exo inhibited cell migration

TGF-β2-induced EMT has been experimented in numerous cell lines as fibrosis models, and ARPE19 cells are one of the leading effector cells in subretinal fibrosis(26, 27). Hence, different concentrations of TGF-β2 were added to ARPE19 cell mediums to establish a successful RPE EMT model and further to verify the roles of hucMSC-Exo under the subretinal fibrosis environment. When ARPE-19 cells were supplied with diverse concentrations of TGF-β2 for 48 h, the epithelial markers expression was downregulated, whereas expression of mesenchymal markers, such as N-cadherin, Vimentin, and α-SMA, were upregulated in protein level (Fig. 4a, b). Stimulation of ARPE-19 cells with TGF-β2 at 10ng/ml resulted in a significant morphological alteration, with a transition from typical cobblestone-like cells to an elongated spindle-shaped mesenchymal-like cells (Fig. 4c). Compared with control group, the stimulated cells displayed a loss of epithelial characteristics and the acquisition of mesenchymal characteristics under the immunofluorescence microscope (Fig. 4d). These results suggested that ARPE-19 cells undergone a process of EMT after treatment with 10 ng/mL TGF-β2.

Additionally, Scratch assays showed that cells treated with TGF-β2 exhibited an enhanced migratory ability, while cells treated with MSC-derived exosomes exerted an opposite effect after 24 and 48 h ($P < 0.05$) (Fig. 4e). Similar results were observed in transwell assay, indicating that fewer cells migrated through the membrane in the hucMSC-Exo group than in the TGF-β2-treated groups after 12 h of incubation (Fig. 4f). These assays consistently demonstrated that exosomes derived from MSC treatment significantly inhibited cell migration.

hucMSC-Exo inhibited the expression of EMT-associated proteins

The alteration of representative proteins is an important feature of RPE cells under the subretinal fibrosis environment. The expression of EMT-related indicators and cell adhesion markers were examined to evaluate the effect of hucMSC-Exo in ARPE19 cells. Immunofluorescence results revealed that the

expression of intercellular tight junction ZO-1 was abrogated by TGF-β2, which was alleviated by hucMSC-Exo. The mesenchymal proteins α-SMA and vimentin were distributed around the cells because of TGF-β2 induction. However, their expression markedly decreased upon exposure to hucMSC-Exo in combination with TGFβ2 compared with the TGF-β2 alone group (Fig. 5a). Besides, hucMSC-Exo significantly upregulated the expression of occludin while decreasing the expression of mesenchymal markers (Vimentin, N-cadherin, and α-SMA) compared with the TGF-β2 group (Fig. 5b). The aforementioned results indicated that hucMSC-Exo reduced subretinal fibrosis through suppressing EMT.

Detection of miR-27b expression in hucMSC-Exo

Studies have shown that miRNAs are enriched in MSC-derived exosomes and play a pivotal role in cellular communication. The present study aimed to identify the miRNAs that contribute to the therapeutic effects of hucMSC-Exo on subretinal fibrosis. We found that eight miRNAs were widely reported to be a strong enrichment in hucMSC-Exo and closely correlated with fibrosis (Fig. 6a). Next, the expression of these miRNAs was detected using qRT-PCR. The results indicated that miR-27b-3p expression was the highest in hucMSC-Exo relative to HSF-Exo (Fig. 6b). The average miR-27b levels relative to U6 in hucMSC-Exo after treatment with RNase (0.5 μg/μL) and 0.1% Triton X-100 for 30 min were measured by qRT-PCR, which verified the presence of miR-27b in hucMSC-Exo. As shown in Figure 6C, exosomes treated with RNase did not show a significantly low level of miR-27b unless they were co-treated with Triton X-100, which degraded the exosomes membrane (Fig. 6c). Hence, miR-27b was protected within the intact exosomes from RNase degradation, which was considered to be a real EV-miRNA. Furthermore, the elevated levels of miR-27 were confirmed in hucMSC-Exo. Therefore, miR-27b-3p was selected as a potential candidate to mediate the therapeutic effects of hucMSC-Exo in the model.

hucMSC-Exo transferred a high level of miR-27b to ARPE19 cells

ARPE19 cells treated with exosomes were transfected with an miR-27b-3p inhibitor (antagomiR-27b-3p) to explore the effect of miR-27b-3p in hucMSC-Exo on TGFβ2-induced ARPE-19 cells. The results showed a marked decline in miR-27b-3p expression following antagomiR-27b-3p transfection (Fig. 7a). Therefore, the study confirmed that transferring miR-27b-3p was one of the mechanisms for hucMSC-Exo to suppress TGF-β2-meditated EMT in ARPE19 cells. The transfection with antagomiR-27b-3p led to a downregulation of epithelial marker occludin, while increasing the expression of mesenchymal markers (Vimentin, N-cadherin, and α-SMA) when compared with the hucMSC-Exo group (Fig. 7b). Consistently, scratch and transwell assays also confirmed that the migration of cells treated with hucMSC-Exo was enhanced if they were also transfected with antagomiR-27b-3p (Fig. 7d, e). The study similarly confirmed that hucMSC-Exo enhanced the expression of tight junction ZO-1 destroyed by TGF-β2, and this effect was eliminated by additional antagomiR-27b-3p treatment. In addition, the expression of mesenchymal proteins α-SMA and Vimentin significantly was increased upon exposure to antagomiR-27b-3p compared with the control group, as detected by immunofluorescence (Fig. 7c). Together, these results revealed that hucMSC-Exo was enriched in miR-27b-3p, which could regulate the functionality of TGFβ2-induced ARPE-19 cells.

Enhancing the expression of miR-27b inhibited TGFβ2-induced EMT

To gain insights into whether miR-27b-3p could exert an impact on TGF-β2-induced EMT, series of experiments were conducted. First, the transfection efficiency of agomiR-27b-3p was detected by qRT-PCR (Fig. 8a). In addition, the addition of miR-27b-3p markedly rescued the loss of epithelial phenotype ZO-1 and inhibited the EMT of ARPE19 cells compared with the TGF-β2 group, as demonstrated by immunofluorescence and western blot analysis (Fig.8b, c). Furthermore, the activation of TGF-β2–induced migration was obviously suppressed by miR-27b-3p overexpression in comparison with that in RPE cells without miR-27b-3p pretreatment (Fig. 8d, e). Together, our results confirmed that miR-27b-3p could directly inhibit the EMT of TGFβ2-induced ARPE19 cells *in vitro*.

Identification of candidate genes regulated by miR-27b

As miR-27b markedly suppressed EMT *in vitro*, the present study concentrated on explicating the potential target of miR-27b in RPE cells. Bioinformatics analysis was performed with five online analysis instruments (miRanda, miRTarbase, TargetScan, miRDB, and miRsystem). As a result, 7 genes were predicted to be direct targets of miR-27b-3p, including HOXC6 (Figure 9a). Among the predicted target genes, the previous literatures have reported that HOXC6 could act as a vital role in EMT(28-30), therefore we chose it as the candidate. In addition, the dual-luciferase reporter assay was applied to confirm whether HOXC6 was a target for miR-27b-3p. The results illustrated that miR-27b-3p overexpression inhibited the luciferase activity of psiCHECK-2-HOXC6-WT, but it did not affect the luciferase activity of psiCHECK-2-HOXC6-MT (Fig. 9b). These data indicated that HOXC6 was a binding target of miR-27b-3p. Consistently, western blot analysis indicated that the expression of HOXC6 was significantly downregulated in ARPE19 cells following transfection with miR-27b-3p mimics while exerted the opposite effect in ARPE19 cells transfected with miR-27b-3p inhibitor (Fig. 9c), which illustrated that HOXC6 was a direct target of miR-27b-3p.

Discussion

Subretinal fibrosis defines the end stage of nAMD, leading to irreversible vision loss; Currently there is no available treatment to either prevent it or treat it. (1). Thus, novel therapeutic methods need to be urgently developed to prevent vision loss and reduce subretinal scar formation in nAMD. Intravitreal administration of MSC has been reported to have an encouraging therapeutic effect on multiple retinal disease models, including retinal damage, inflammation, and nerve injury (23). Despite the beneficial effects of MSCs in repairing retinal injury and restoring the visual system, their application is confined to ethical issues, poor diffusion through biological barriers and possible complications such as epiretinal membranes, inflammatory response and malignant transformation (31). It is now clear that they exert most of their biological effects through the paracrine secretion of soluble factors and exosomes (21). Exosomes derived from MSCs have been shown to own all the superiority of MSCs in limiting the extent of damage, reducing apoptosis and restricting inflammation (16, 20, 32). Importantly, exosomes have a reliable stability, a better ability to penetrate deep tissues and avoid immune attack, a lower chance of

immunological rejection, and no risk of malignant transformation or vitreoretinal proliferation and uncertain differentiation in MSCs (33, 34).

MicroRNA, a class of small noncoding RNAs, serves as a regulator of gene expression at the post-transcriptional level, causing a translational arrest or mRNA degradation(35). They are involved in regulating basic cellular processes such as proliferation and differentiation(36). In addition, many studies analyzed the miRNA disorders in patients with AMD which suggested that the miRNA-based treatment may put forward a promising novel strategy to ameliorate AMD-related tissue damage (37).Our preliminary literature screening and PCR results indicated that miR-27b-3p from hucMSC-Exo might be one of the critical miRNAs in subretinal fibrosis. MiR-27b was discovered to be observably upregulated in nAMD plasma, and upregulation of miR-27b markedly blocked the cell proliferation and migration in PDGF-BB-induced ARPE19 cells (38, 39). Although various growth factors, including platelet-derived growth factor (PDGF), hepatocyte growth factor(HGF), connective tissue growth factor (CTGF) and transforming growth factor-β (TGF-β) are involved in the pathogenesis, our present study focused on TGF-β2 because it is predominant in aqueous humor and its concentration in the vitreous humor has a correlation with the progression of retinal fibrosis. Moreover, PDGF, TGF-β1, and CTGF are known to be targets of TGF-β2 signaling, implying that TGF-β2 can coordinate the secondary effects of these other factors on EMT and fibrosis (40).Importantly, previous studies have demonstrated that suppression of TGF-β2-induced EMT could reduce the development of collagen fibers and fibrotic membrane and thereby against fibrosis-relative retinal diseases(41),and there is no relevant report showing that miR-27b is involved in the EMT of RPE cells induced by TGF-β2. Therefore, we aimed to explore the effects of hucMSC-Exo and its containing miR-27b on subretinal fibrosis *in vivo* and *in vitro* and further investigated its anti-fibrotic mechanism.

This study was novel in demonstrating that hucMSC-Exo had the ability to alleviate subretinal fibrosis, including the decrease in both CNV and subretinal fibrosis, the reduction of migration, and the reversal of EMT markers in TGF-β2-induced RPE cells. Moreover, we found that hucMSC-Exo inhibited subretinal fibrosis by the delivery of miR-27b because when silencing the expression of miR-27b in hucMSC-Exo, the inhibitory effects were weakened, but it was rescued after miR-27b overexpression. Bioinformatics analysis and luciferase reporter assay revealed that miR-27b-3p directly targeted the 3'-UTR of HOXC6. Consistently, upregulation of miR-27b-3p markedly downregulated HOXC6 expression at the protein level($P<0.05$). HOXC6, a member of the homeobox superfamily, plays pivotal roles in numerous cellular processes, including cell apoptosis, proliferation and differentiation (42). Studies have shown that silencing of HOXC6 suppressed EMT via the inhibition of the TGF-β/Smad signaling pathway in cervical carcinoma cells (28). Therefore, miR-27b-3p is likely to block the activation of the TGF-β/Smad signaling pathway in RPE cells partly by targeting HOXC6 gene.

This study had several limitations. Firstly, miR-27b-3p is just one of the significantly increased miRNAs in hucMSC-Exo compared with HSF-exosomal miRNAs. Although hucMSC-Exo strongly inhibited the activation of EMT in RPE cells and reduced subretinal fibrosis, the roles of other miRNAs also deserve further investigation. Secondly, although the experiments strongly demonstrated that miR-27b-3p had an

obvious inhibitory effect on the EMT of ARPE19 cells, the same effect in animals needs to be further verified. Finally, a large amount of studies have demonstrated that miRNAs packaged in MSC-Exos were functional molecules mediated beneficial effects (43), but the therapeutic effect of proteins and other beneficial components also deserves further research. In brief, we believe that exosomes derived from MSCs have a great potential to be superior candidates in the therapy of retina diseases in various clinical stages and an in-depth study about its whole effect and mechanism are needed in the future.

Conclusions

hucMSC-derived miR-27-3p-enriched exosomes effectively suppressed the activation of EMT in RPE cells and alleviated subretinal fibrosis by inhibiting the process of EMT in TGFβ2-treated RPE cells. The present study provided a possible therapeutic tool for treating fibrosis-related retinal disease, as well as insights into the mechanism of hucMSC-Exo in subretinal fibrosis.

Abbreviations

ARVO: Association for Research in Vision and Ophthalmology

α-SMA: α-smooth muscle actin

CNV: choroidal neovascularization

CTGF: connective tissue growth factor

DMEM: Dulbecco's modified Eagle medium

EMT: epithelial-mesenchymal transition

HucMSCs-Exo: human umbilical cord mesenchymal stem cell-derived exosomes

H&E: hematoxylin and eosin

HGF: hepatocyte growth factor

MSC: mesenchymal stem cell

nAMD: neovascular age-related macular degeneration

PFA: Paraformaldehyde

PDGF: platelet-derived growth factor

RPE: Retinal pigmented epithelium

TEM: transmission electron microscopy

Declarations

Availability of data and materials

The authors confirm that the data supporting the findings of this study are available within the article.

Acknowledgements

We would like to acknowledge the colleagues for their helpful assistance on this study.

Funding

This work was supported by the National Key R&D Program of China (grant Nos.2016YFC0904800,2019YFC0840607), National Science and Technology Major Project of China (grant Nos.2017ZX09304010), Shanghai Science and Technology Commission Research Project (grant Nos.19401932700) and Clinical Research Innovation Plan of Shanghai General Hospital (grant Nos. CTCCR-2018BP04), Bethune Lumitin Reasarch Funding for the young and middle-aged Ophthalmologists (BJ-LM2016003J).

Author information

Affiliations

Department of Ophthalmology, Shanghai General Hospital, Shanghai Jiao Tong University School of Medicine, National Clinical Research Center for Eye Diseases, Shanghai Key Laboratory of Ocular Fundus Diseases, Shanghai Engineering Center for Visual Science and Photomedicine, Shanghai engineering center for precise diagnosis and treatment of eye diseases; NO.100, Haining Road, Hongkou District, Shanghai, China, 200080

Dongli Li, Junxiu Zhang, Liuzi Jia, Qing Gu, Yuanyuan Gong & Zhi Zheng

Contributions

YG, DL and ZZ conceived and designed the study.DL conducted the experiments, interpreted the data, and prepared the manuscript. JZ made the animal models. QG performed the cell culture. All authors read and approved the final manuscript.

Corresponding authors

Correspondence to Yuanyuan Gong or Zhi Zheng.

Ethics declarations

Ethics approval and consent to participate

This study was approved by the ethics committee of the First Affiliated Hospital of Zhengzhou University(Approval No. 20180301). The informed consent of the patients was obtained, and this study was performed following the principles recommended by the Declaration of Helsinki. All experimental procedures involving animals were performed in accordance with animal protocols approved by the Institutional Animal Use and Care Committee.

Consent for publication

Not applicable.

Competing interests

The authors declare no conflicts of interest related to the studies described..

Publisher's Note

Springer Nature remains neutral with regard to jurisdictional claims in published maps and institutional affiliations.

References

1. Ishikawa K, Kannan R, Hinton DR. Molecular mechanisms of subretinal fibrosis in age-related macular degeneration. Exp Eye Res. 2016;142:19-25.
2. Wu D, Kanda A, Liu Y, Kase S, Noda K, Ishida S. Galectin-1 promotes choroidal neovascularization and subretinal fibrosis mediated via epithelial-mesenchymal transition. FASEB J. 2019;33(2):2498-513.
3. Shu DY, Butcher E, Saint-Geniez M. EMT and EndMT: Emerging Roles in Age-Related Macular Degeneration. Int J Mol Sci. 2020;21(12).
4. Rossato FA, Su Y, Mackey A, Ng YSE. Fibrotic Changes and Endothelial-to-Mesenchymal Transition Promoted by VEGFR2 Antagonism Alter the Therapeutic Effects of VEGFA Pathway Blockage in a Mouse Model of Choroidal Neovascularization. Cells. 2020;9(9).
5. Nagai N, Suzuki M, Uchida A, Kurihara T, Kamoshita M, Minami S, et al. Non-responsiveness to intravitreal aflibercept treatment in neovascular age-related macular degeneration: implications of serous pigment epithelial detachment. Sci Rep. 2016;6:29619.
6. Hwang JC, Del Priore LV, Freund KB, Chang S, Iranmanesh R. Development of subretinal fibrosis after anti-VEGF treatment in neovascular age-related macular degeneration. Ophthalmic Surg Lasers Imaging. 2011;42(1):6-11.
7. Daniel E, Toth CA, Grunwald JE, Jaffe GJ, Martin DF, Fine SL, et al. Risk of scar in the comparison of age-related macular degeneration treatments trials. Ophthalmology. 2014;121(3):656-66.
8. Casalino G, Stevenson MR, Bandello F, Chakravarthy U. Tomographic Biomarkers Predicting Progression to Fibrosis in Treated Neovascular Age-Related Macular Degeneration: A Multimodal

Imaging Study. Ophthalmol Retina. 2018;2(5):451-61.

9. Shimizu H, Yamada K, Suzumura A, Kataoka K, Takayama K, Sugimoto M, et al. Caveolin-1 Promotes Cellular Senescence in Exchange for Blocking Subretinal Fibrosis in Age-Related Macular Degeneration. Invest Ophthalmol Vis Sci. 2020;61(11):21.
10. Mettu PS, Allingham MJ, Cousins SW. Incomplete response to Anti-VEGF therapy in neovascular AMD: Exploring disease mechanisms and therapeutic opportunities. Prog Retin Eye Res. 2020:100906.
11. Uder C, Bruckner S, Winkler S, Tautenhahn HM, Christ B. Mammalian MSC from selected species: Features and applications. Cytometry A. 2018;93(1):32-49.
12. Zhao G, Ge Y, Zhang C, Zhang L, Xu J, Qi L, et al. Progress of Mesenchymal Stem Cell-Derived Exosomes in Tissue Repair. Curr Pharm Des. 2020;26(17):2022-37.
13. Li D, Gong Y. A Promising Strategy for Non-Arteritic Anterior Ischemic Optic Neuropathy: Intravitreal Mesenchymal Stem Cell Exosome. Curr Stem Cell Res Ther. 2020.
14. Vlassov AV, Magdaleno S, Setterquist R, Conrad R. Exosomes: current knowledge of their composition, biological functions, and diagnostic and therapeutic potentials. Biochim Biophys Acta. 2012;1820(7):940-8.
15. Mathieu M, Martin-Jaular L, Lavieu G, Thery C. Specificities of secretion and uptake of exosomes and other extracellular vesicles for cell-to-cell communication. Nat Cell Biol. 2019;21(1):9-17.
16. Mead B, Amaral J, Tomarev S. Mesenchymal Stem Cell-Derived Small Extracellular Vesicles Promote Neuroprotection in Rodent Models of Glaucoma. Invest Ophthalmol Vis Sci. 2018;59(2):702-14.
17. Ma M, Li B, Zhang M, Zhou L, Yang F, Ma F, et al. Therapeutic effects of mesenchymal stem cell-derived exosomes on retinal detachment. Exp Eye Res. 2020;191:107899.
18. Zhang W, Wang Y, Kong Y. Exosomes Derived From Mesenchymal Stem Cells Modulate miR-126 to Ameliorate Hyperglycemia-Induced Retinal Inflammation Via Targeting HMGB1. Invest Ophthalmol Vis Sci. 2019;60(1):294-303.
19. He GH, Zhang W, Ma YX, Yang J, Chen L, Song J, et al. Mesenchymal stem cells-derived exosomes ameliorate blue light stimulation in retinal pigment epithelium cells and retinal laser injury by VEGF-dependent mechanism. Int J Ophthalmol. 2018;11(4):559-66.
20. Mead B, Ahmed Z, Tomarev S. Mesenchymal Stem Cell-Derived Small Extracellular Vesicles Promote Neuroprotection in a Genetic DBA/2J Mouse Model of Glaucoma. Invest Ophthalmol Vis Sci. 2018;59(13):5473-80.
21. Yu B, Zhang X, Li X. Exosomes derived from mesenchymal stem cells. Int J Mol Sci. 2014;15(3):4142-57.
22. Mathew B, Ravindran S, Liu X, Torres L, Chennakesavalu M, Huang CC, et al. Mesenchymal stem cell-derived extracellular vesicles and retinal ischemia-reperfusion. Biomaterials. 2019;197:146-60.
23. Nuzzi R, Caselgrandi P, Vercelli A, Cantore S. Effect of Mesenchymal Stem Cell-Derived Exosomes on Retinal Injury: A Review of Current Findings. Stem Cells International. 2020;2020:1-9.

24. Yu B, Shao H, Su C, Jiang Y, Chen X, Bai L, et al. Exosomes derived from MSCs ameliorate retinal laser injury partially by inhibition of MCP-1. Sci Rep. 2016;6:34562.
25. Busser H, Najar M, Raicevic G, Pieters K, Velez Pombo R, Philippart P, et al. Isolation and Characterization of Human Mesenchymal Stromal Cell Subpopulations: Comparison of Bone Marrow and Adipose Tissue. Stem Cells Dev. 2015;24(18):2142-57.
26. Connor TB, Jr., Roberts AB, Sporn MB, Danielpour D, Dart LL, Michels RG, et al. Correlation of fibrosis and transforming growth factor-beta type 2 levels in the eye. J Clin Invest. 1989;83(5):1661-6.
27. Kobayashi M, Tokuda K, Kobayashi Y, Yamashiro C, Uchi SH, Hatano M, et al. Suppression of Epithelial-Mesenchymal Transition in Retinal Pigment Epithelial Cells by an MRTF-A Inhibitor. Invest Ophthalmol Vis Sci. 2019;60(2):528-37.
28. Zhang F, Ren CC, Liu L, Chen YN, Yang L, Zhang XA. HOXC6 gene silencing inhibits epithelial-mesenchymal transition and cell viability through the TGF-beta/smad signaling pathway in cervical carcinoma cells. Cancer Cell Int. 2018;18:204.
29. Li PD, Chen P, Peng X, Ma C, Zhang WJ, Dai XF. HOXC6 predicts invasion and poor survival in hepatocellular carcinoma by driving epithelial-mesenchymal transition. Aging (Albany NY). 2018;10(1):115-30.
30. You X, Zhou Z, Chen W, Wei X, Zhou H, Luo W. MicroRNA-495 confers inhibitory effects on cancer stem cells in oral squamous cell carcinoma through the HOXC6-mediated TGF-beta signaling pathway. Stem Cell Res Ther. 2020;11(1):117.
31. Ding SLS, Kumar S, Mok PL. Cellular Reparative Mechanisms of Mesenchymal Stem Cells for Retinal Diseases. Int J Mol Sci. 2017;18(8).
32. Mead B, Tomarev S. Bone Marrow-Derived Mesenchymal Stem Cells-Derived Exosomes Promote Survival of Retinal Ganglion Cells Through miRNA-Dependent Mechanisms. Stem Cells Transl Med. 2017;6(4):1273-85.
33. Kim JY, You YS, Kim SH, Kwon OW. EPIRETINAL MEMBRANE FORMATION after INTRAVITREAL AUTOLOGOUS STEM CELL IMPLANTATION in A RETINITIS PIGMENTOSA PATIENT. Retinal Cases and Brief Reports. 2017;11(3):227-31.
34. Huang H, Kolibabka M, Eshwaran R, Chatterjee A, Schlotterer A, Willer H, et al. Intravitreal injection of mesenchymal stem cells evokes retinal vascular damage in rats. FASEB journal : official publication of the Federation of American Societies for Experimental Biology. 2019;33(12):14668-79.
35. Jonas S, Izaurralde E. Towards a molecular understanding of microRNA-mediated gene silencing. Nat Rev Genet. 2015;16(7):421-33.
36. Wang SS, Wang C, Chen H. MicroRNAs are critical in regulating smooth muscle cell mineralization and apoptosis during vascular calcification. J Cell Mol Med. 2020.
37. Berber P, Grassmann F, Kiel C, Weber BH. An Eye on Age-Related Macular Degeneration: The Role of MicroRNAs in Disease Pathology. Mol Diagn Ther. 2017;21(1):31-43.
38. Ertekin S, Yildirim O, Dinc E, Ayaz L, Fidanci SB, Tamer L. Evaluation of circulating miRNAs in wet age-related macular degeneration. Mol Vis. 2014;20:1057-66.

39. Li J, Hui L, Kang Q, Li R. Down-regulation of microRNA-27b promotes retinal pigment epithelial cell proliferation and migration by targeting Nox2. Pathol Res Pract. 2018;214(7):925-33.
40. Saika S. TGFbeta pathobiology in the eye. Lab Invest. 2006;86(2):106-15.
41. Chen CL, Chen YH, Tai MC, Liang CM, Lu DW, Chen JT. Resveratrol inhibits transforming growth factor-beta2-induced epithelial-to-mesenchymal transition in human retinal pigment epithelial cells by suppressing the Smad pathway. Drug Des Devel Ther. 2017;11:163-73.
42. Yu M, Zhan J, Zhang H. HOX family transcription factors: Related signaling pathways and post-translational modifications in cancer. Cell Signal. 2020;66:109469.
43. Pegtel DM, Gould SJ. Exosomes. Annu Rev Biochem. 2019;88:487-514.

Figures

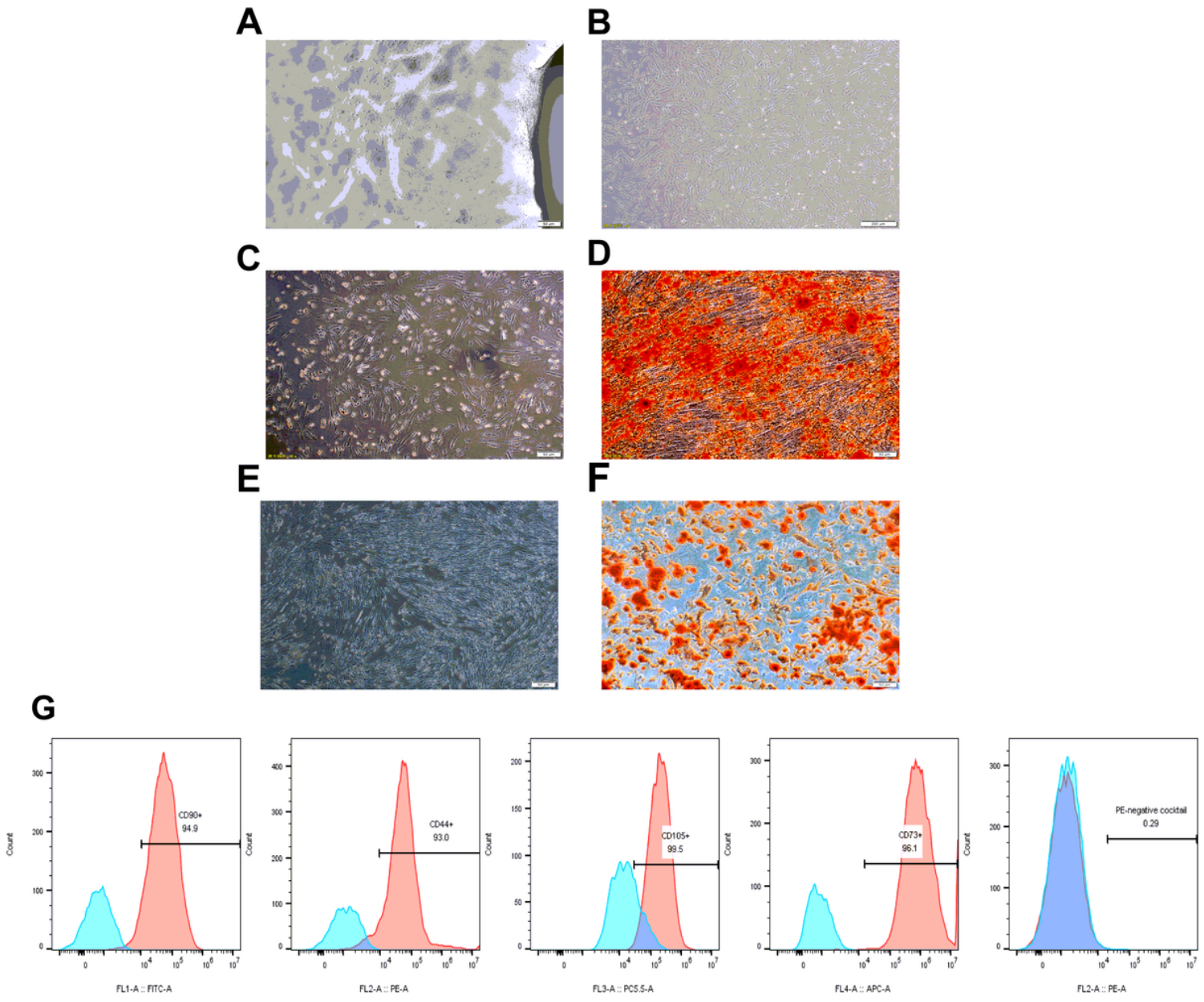

Figure 1

Characteristics of hucMSCs. a, b Cell morphology of passage 0 (bar = 50 μm) and passage 3 (bar = 200 μm) human umbilical cord mesenchymal stem cells (hucMSCs) observed under an inverted microscope (bar = 50 μm). c,d Osteogenic differentiation of hucMSCs was performed in the differentiation medium, while the control cells were grown in a regular medium; Both of them were dyed with Alizarin Red S staining. Most hucMSCs were Alizarin red positive. e , f Oil red O staining was used to stain hucMSCs after adipogenic differentiation, showing the Oil red O–positive lipid droplets. g Flow cytometry analysis of the phenotypic markers of hucMSCs showed that hucMSCs were positive for CD90, CD44, CD105, CD73, and CD105, and negative for CD34, CD45, CD11b, CD19, and human leukocyte antigen (HLA)-DR.

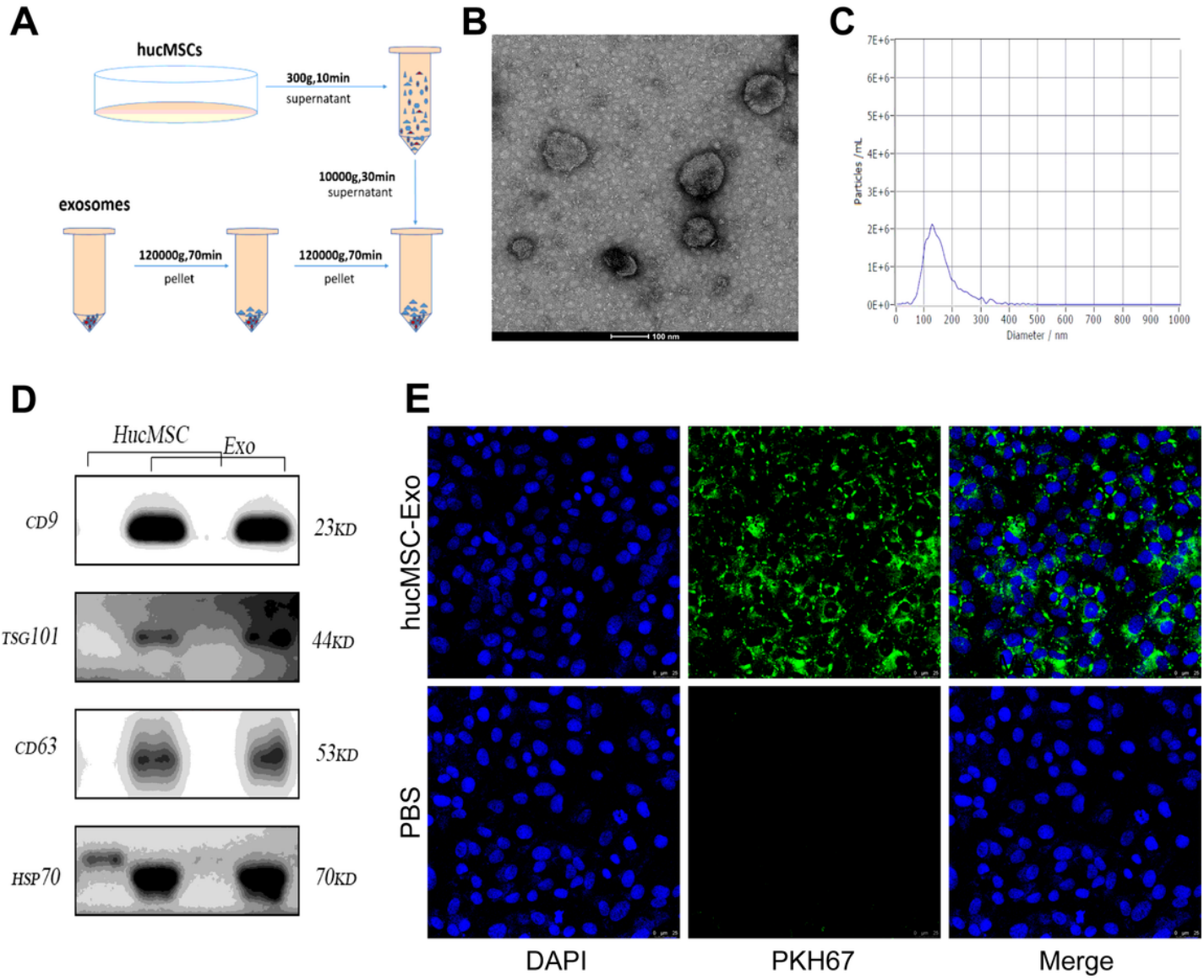

Figure 2

Identification of hucMSC-derived exosomes (hucMSC-Exo). a Method by which hucMSC-Exo were isolated from the conditioned medium using serial centrifugation. b Transmission electron microscopic images of typical hucMSC-Exo. Scale bar = 100 nm. c Size distribution of the hucMSC-Exo was performed using nanoparticle tracking analysis. hucMSC-Exo have an original concentration of 8.8 E+9 particles/mL, a mean size of 159.0 nm, and a peak size of 128.6 nm. d Positive expression of markers

CD9, TSG101, CD63, and HSP70 was mainly detected in hucMSC-Exo using Western blot analysis. e Fluorescence result of ARPE19 cells after being co-cultured with hucMSC-Exo labeled with PKH67, observed under a confocal microscope (scale bar = 25 μm).

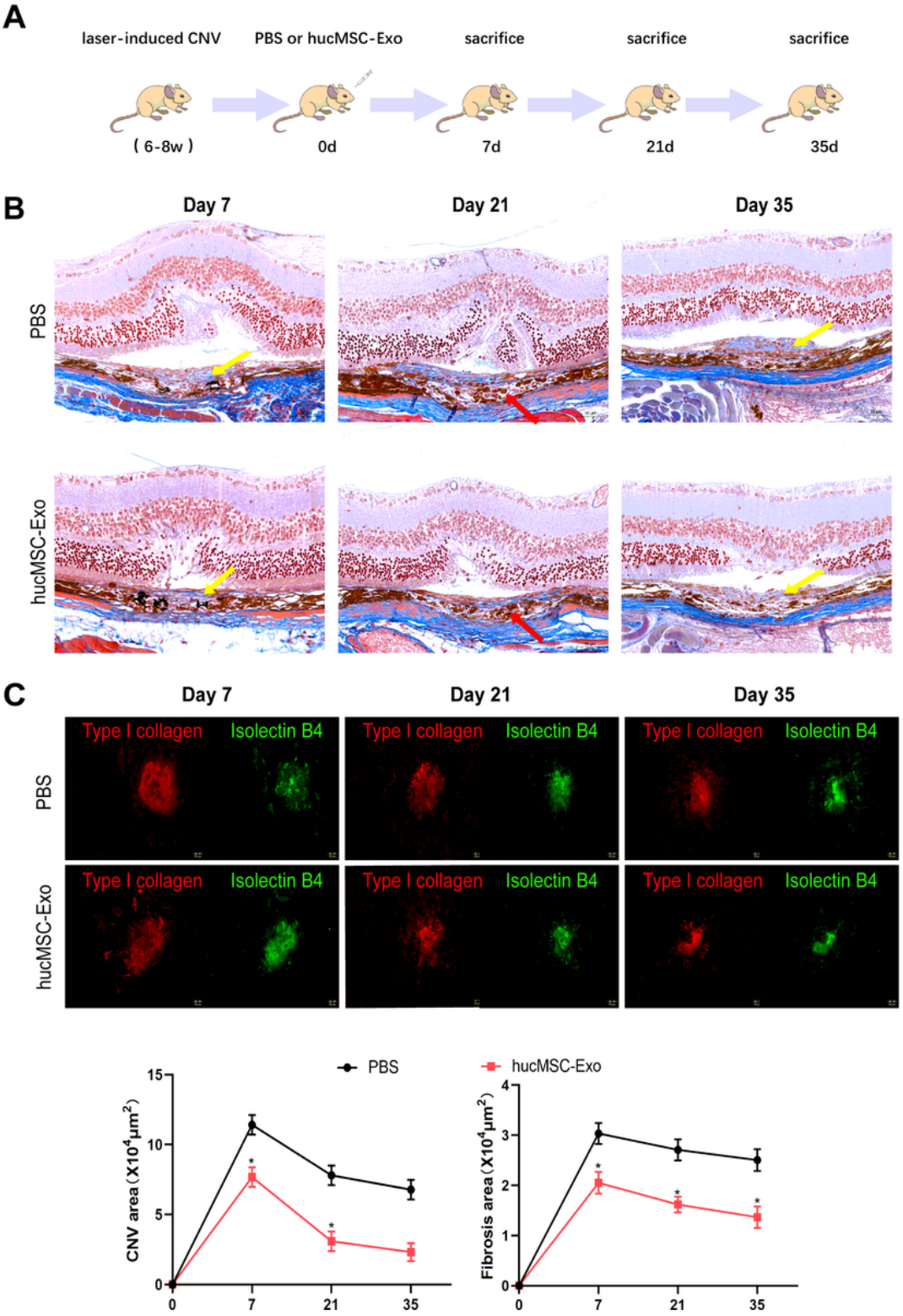

Figure 3

hucMSC-Exo treatment had less fibrosis development in vivo. a Study design. b Normal retina showed a continuous structure. c RPE–Bruch membrane complex was disrupted, and the normal arrangement of

the inner nuclear layer was lost 7 days after the laser burn. d Neovascular hide beneath the subretinal space 7 days after the laser burn. e Compared with the PBS group, collagen fibers were reduced (blue) in the group treated with hucMSC-derived exosomes 35 days after laser photocoagulation. f Choroidal neovascularization (CNV; dyed with isolectin B4) and fibrosis (dyed with collagen type I) were recorded 7, 21, and 35 days after laser burn in the PBS and hucMSC-Exo groups. g Mean volume of the CNV and fibrosis 7, 21, and 35 days after laser burn.

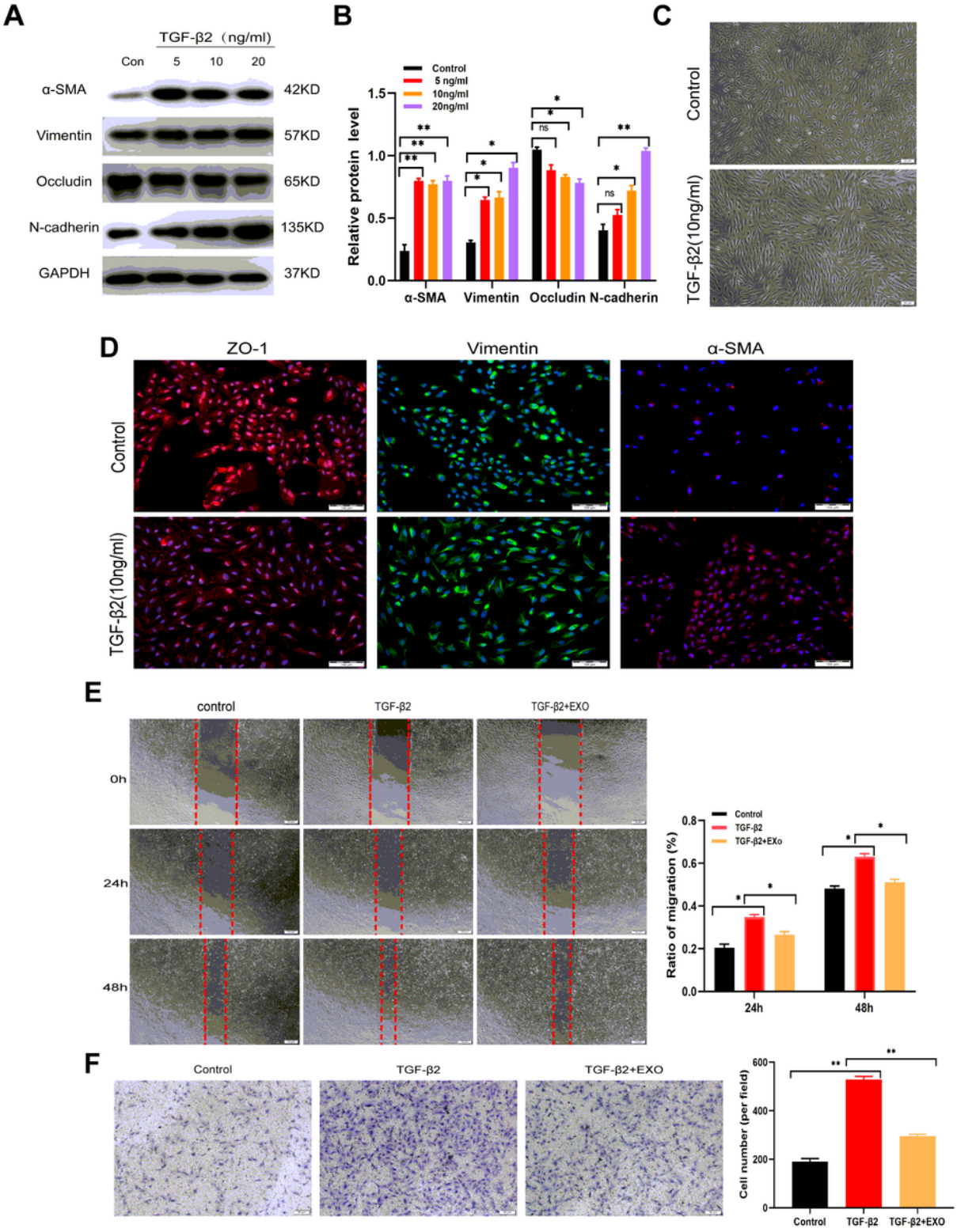

Figure 4

Effects of hucMSC-Exo on cell migration. a, b Effect of different concentrations of hucMSC-Exo on the expression of occludin, Vimentin, N-cadherin, and α-SMA in TGF-β2-treated ARPE19 cells. c Typical morphological alteration of ARPE19 cells in the untreated group or in the 10 ng/mL TGF-β2-treated group. d Immunocytochemistry of ARPE19 cells. The cells were fixed with PFA and dyed with preliminary antibodies against ZO-1, α-SMA, and Vimentin. Scale bar = 20 μm. e Images of cells were recorded at 0, 24, and 48 h after a scratch. Scale bar = 50 μm. f Harvested cells were plated on the upper chamber, migrated for an additional 12 h. The migrated cells were recorded under a phase-contrast microscope. Statistics are presented as means ± SD. *P,0.05, **P < 0.01, ***P < 0.001.

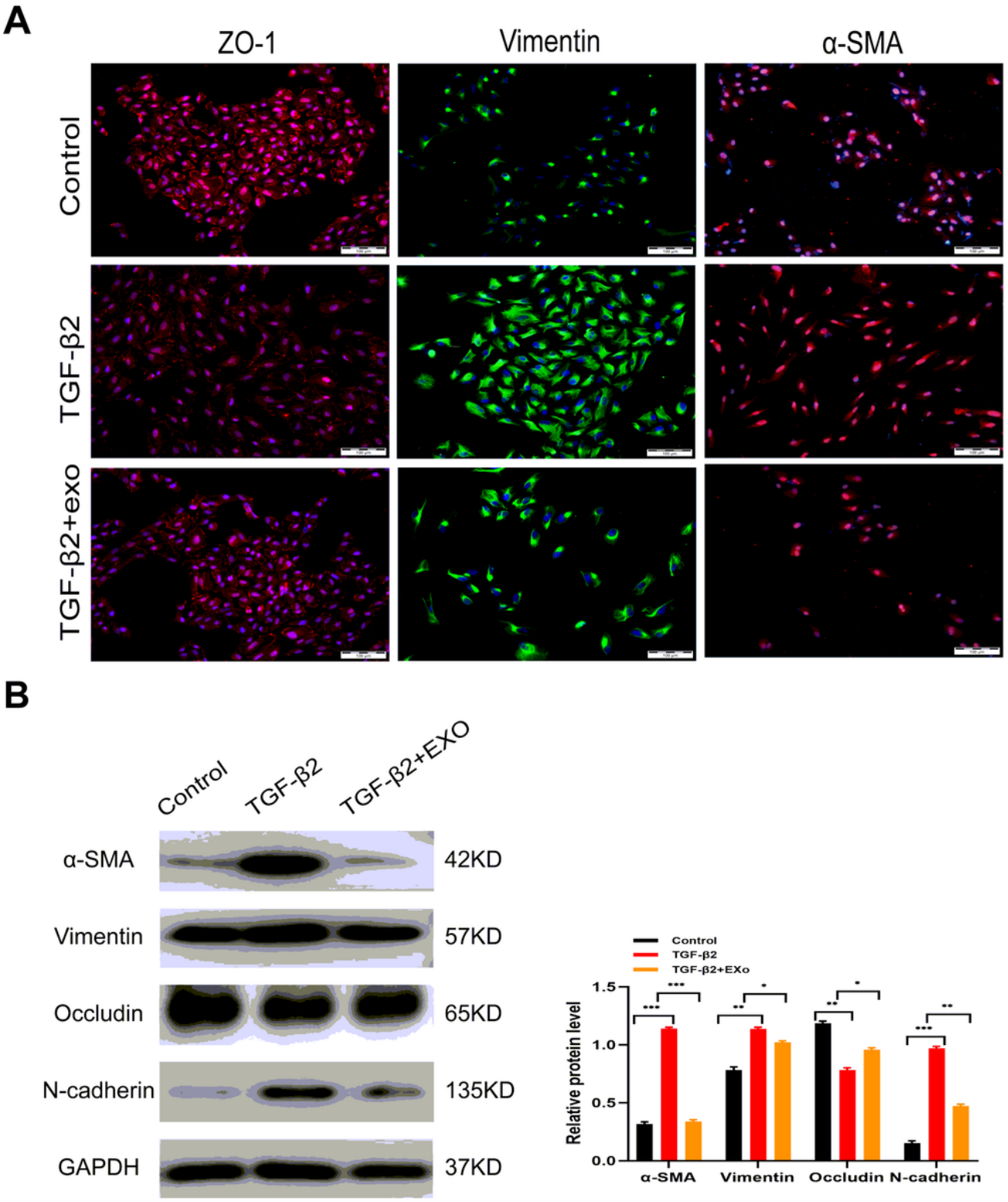

Figure 5

Inhibitory effect of hucMSC-Exo on TGF-β2-treated EMT in ARPE19 cells. a Immunofluorescence staining of Vimentin, ZO-1, and α-SMA expression in ARPE19 cells treated with or without 100 μg/mL hucMSC-Exo; the nuclei were stained with DAPI. b Extracted total protein was loaded and analyzed by Western blot analysis. The relative protein expression was quantified. The data represent the average of three independent experiments. Statistics are presented as means ± SD. *P<0.05, **P < 0.01, ***P < 0.001.

Relative miR-27b-3p expression in exosomes. a Candidate miRNA were screened using the Venn diagram package. b Predictions of eight potential targeted miRNAs of hucMSC-Exo were detected by qRT-PCR; HSF-Exo was used as the reference. Different-color areas represent different datasets. c Average miR-27b levels in hucMSC-Exo after treatments with RNase and Triton X-100 for 30 min, relative to miR-27b levels in the control untreated group, normalized to U6. Statistics are presented as means ± SD. *P,0.05, **P < 0.01, ***P < 0.001.

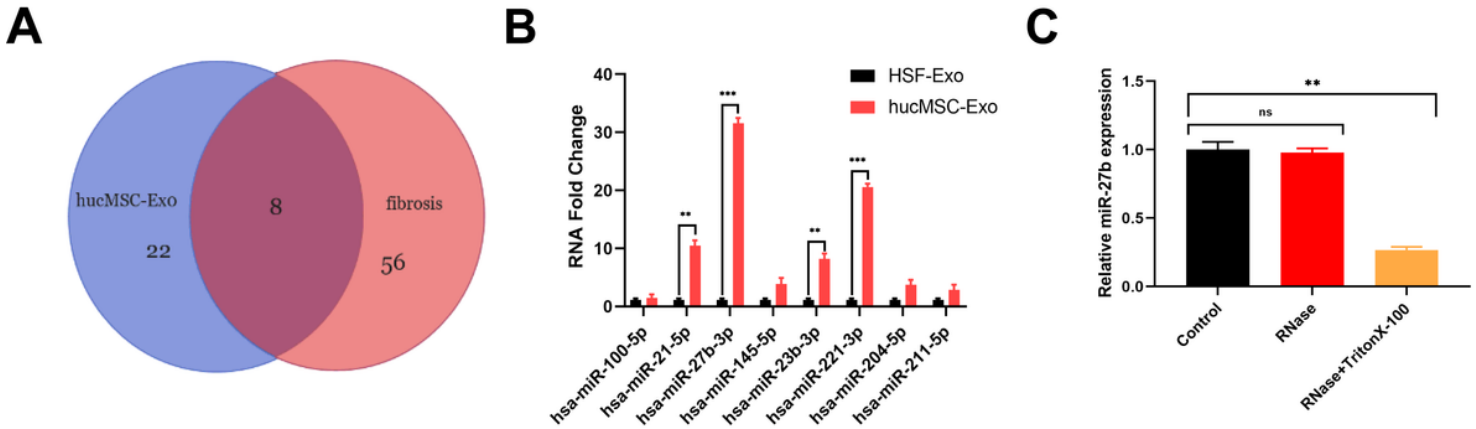

Figure 6

hucMSC-Exo were enriched with miR-27b-3p that could suppress the EMT process. a qRT-PCR showed that the application of antagomiR-27b-3p could counteract the overexpression of miR-27b-3p caused by hucMSC-Exo. b, c Western blot analysis indicated that antagomiR-27b-3p could recover the EMT process suppressed by hucMSC-Exo. d Effect of antagomiR-27b-3p on the EMT-related protein changes assessed by immunofluorescence. e–g Effects of antagomiR-27b-3p on the migration and wound-healing ability of ARPE19 cells were measured by Transwell and scratch assays; hucMSC-Exo were used as a reference. Statistics are presented as means ± SD. *P,0.05, **P < 0.01, ***P < 0.001.

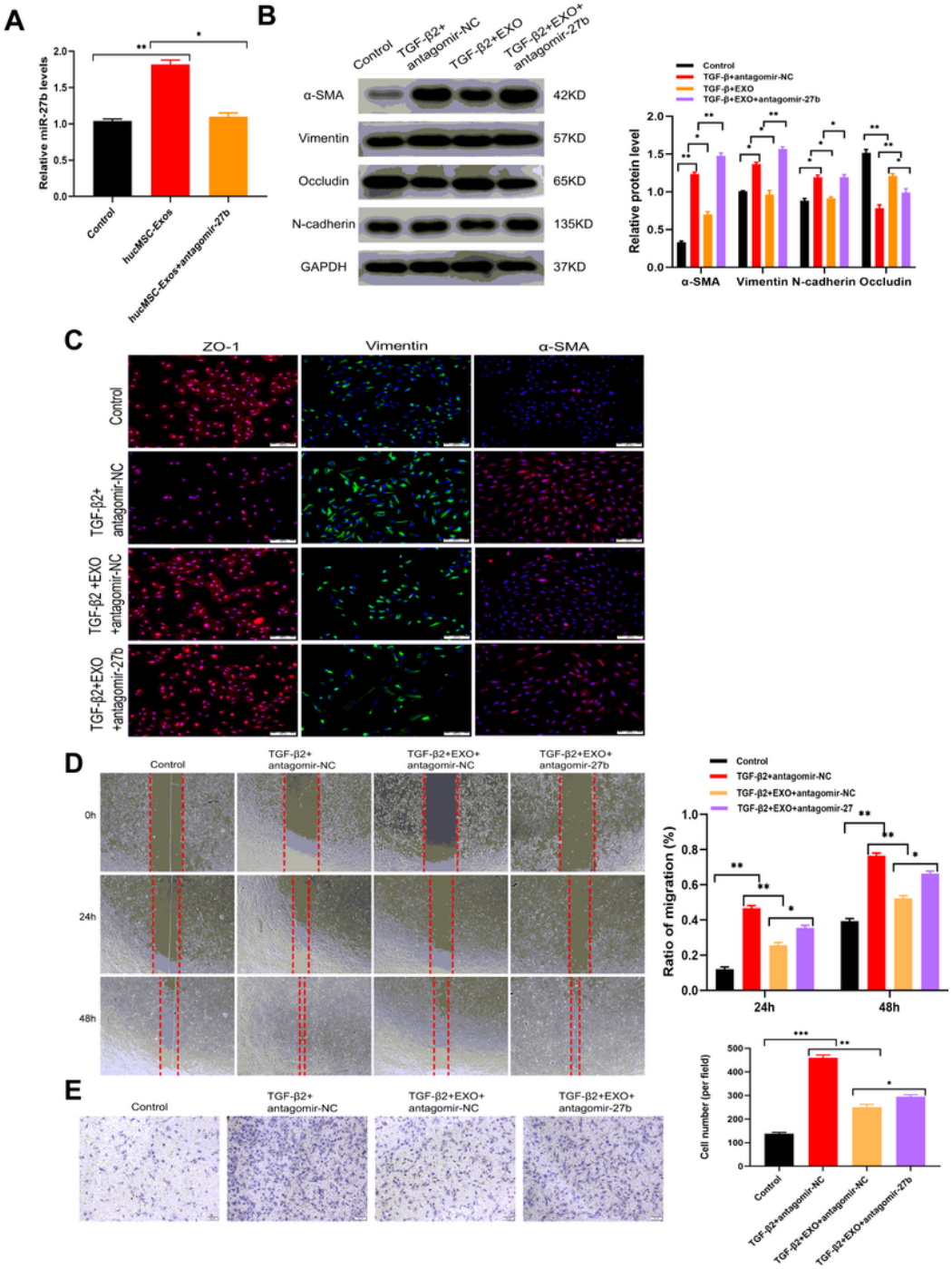

Figure 7

miR-27b-3p inhibited cell migration and expression of EMT-associated proteins in vitro. a miR-27b-3p level in three groups analyzed by qRT-PCR. b, c Effect of miR-27b-3p on the expression of EMT-related proteins occludin, Vimentin, N-cadherin, and α-SMA evaluated by Western blot analysis. d–f Effects of miR-27b-3p on the migration and wound-healing ability of ARPE19 cells. g Immunofluorescence was

further used to assess cell morphological alteration. Statistics are presented as means ± SD. *P<0.05, **P < 0.01, ***P < 0.001.

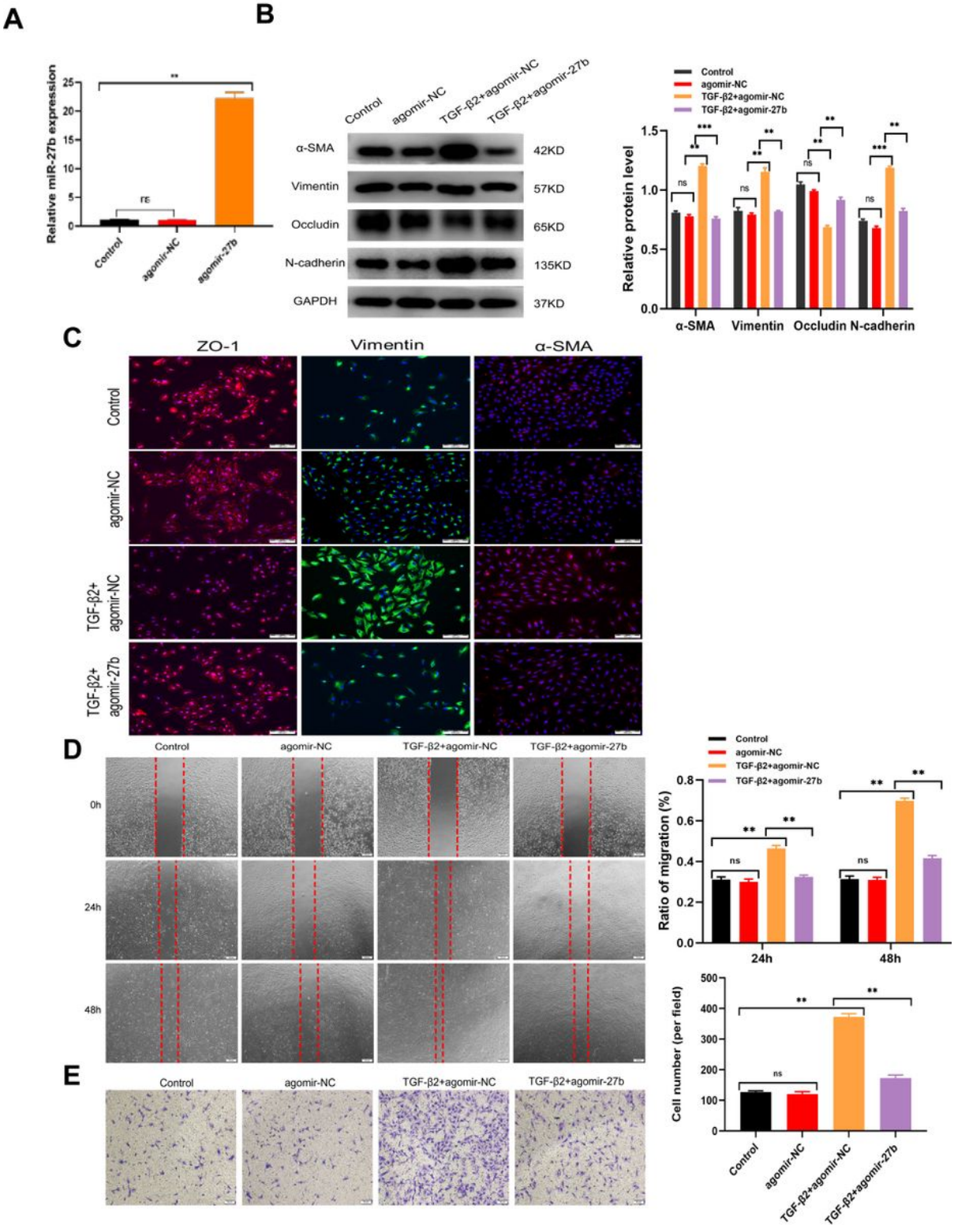

Figure 8

miR-27b-3p modulated the EMT process by suppressing HOXC6. a Potential targets of miR-27b-3p were predicted using five databases (TargetScan, miRanda, miRtarbase, miRSystem, and miRDB). b Targeted binding sites of miR-27b-3p on HOXC6 3′-UTR. c Targeted relationship of miR-27b-3p with HOXC6 was

verified by the dual-luciferase assay. Data are presented as the mean ± SD. **P < 0.01, ***P < 0.001. d Effect of miR-27b-3p on the expression of HOXC6 assessed by Western blot analysis. Data are the means ± SD of three independent experiments. *P < 0.05, **P < 0.01, ***P < 0.001.

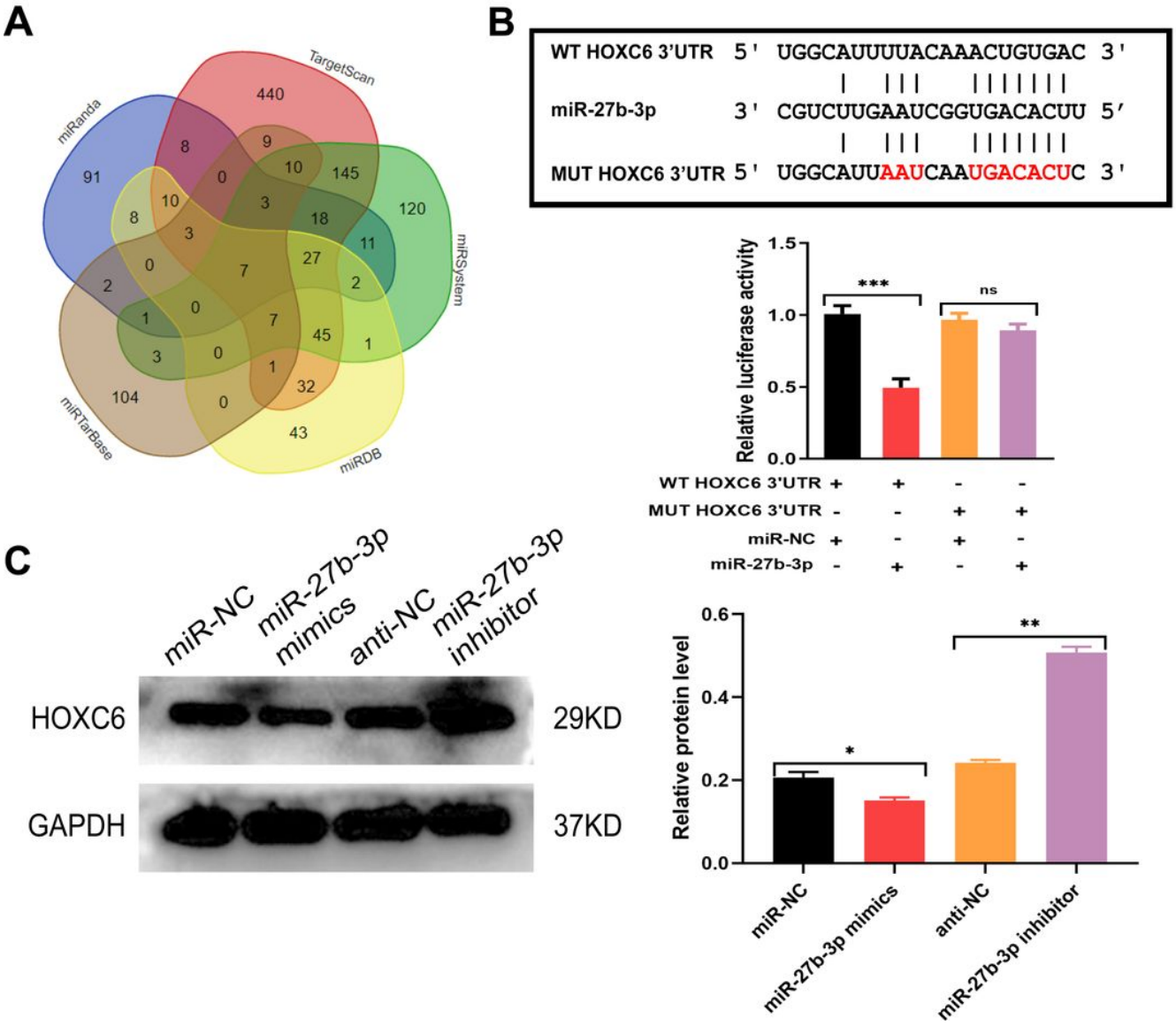

Figure 9

miR-27b-3p modulates EMT process by suppressing HOXC6. a The binding targets of miR-27b-3p was predicted through five database (Targetscan, miRanda, miRtarbase, miRSystem and miRDB. b Targeted binding sites of miR-27b-3p on HOXC6 3UTR; c The targeted relationship of miR-27b-3p with HOXC6 was verified by dual-luciferase assay. d Effect of miR-27b-3p on the expression of HOXC6 assessed by western blotting. Data are the means ± SD three independent experiments. *p < 0.05, **p < 0.01, ***p < 0.001.

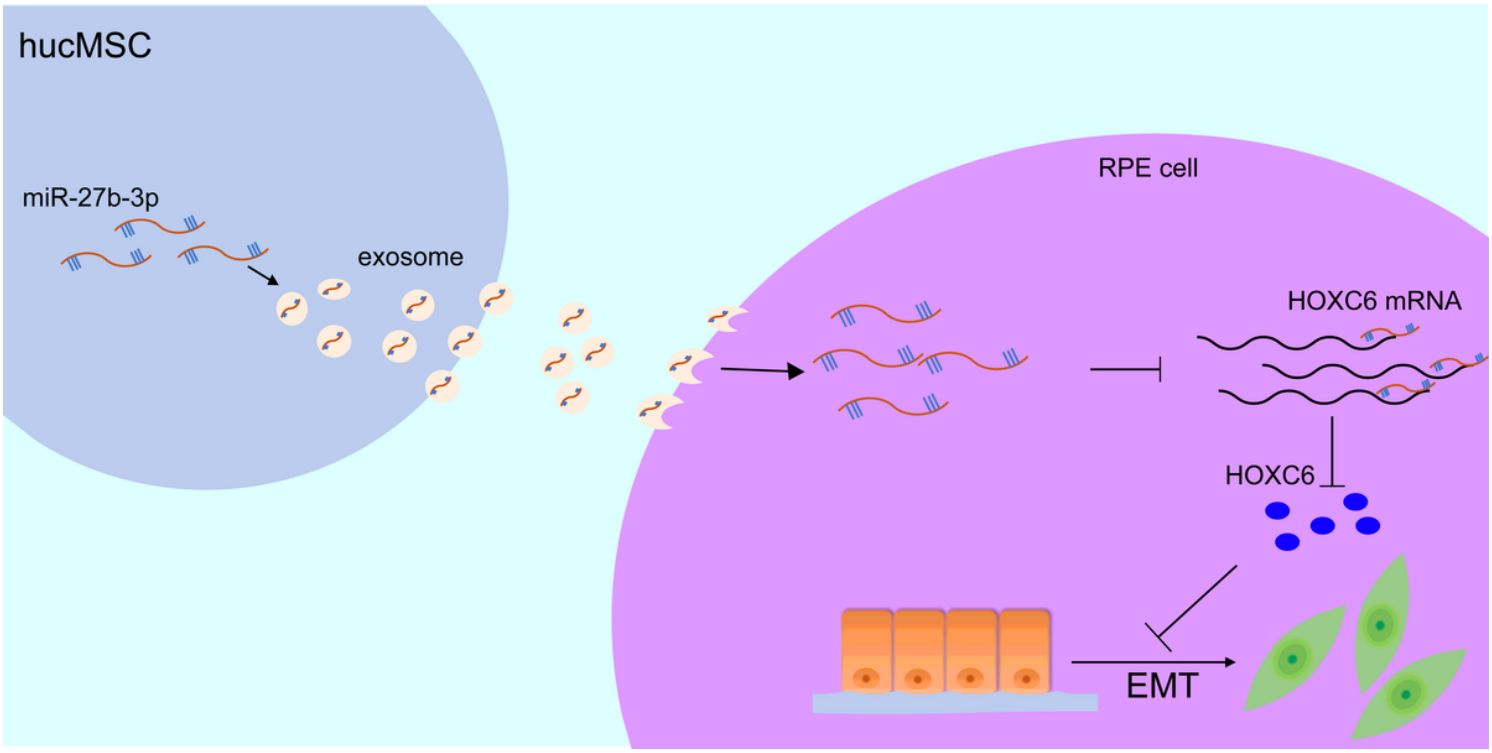

Figure 10

Schematic representation portrays that hucMSC derived exosomal miR-27b-3p could alleviate subretinal fibrosis via suppressing epithelial-mesenchymal transition by targeting hoxc6.